# Optimized deposition of $TiO_2$ thin films produced by a non-aqueous sol-gel method and quantification of their photocatalytic activity

**Charline M. Malengreaux [a,*], Adrien Timmermans [a], Sophie L. Pirard [a], Stéphanie D. Lambert [a], Jean-Paul Pirard [a], Dirk Poelman [b], Benoît Heinrichs [a]**

[a] *Laboratoire de Génie Chimique, B6a, Université de Liège, B-4000 Liège, Belgium*

[b] *LumiLab, Department of Solid State Sciences, Ghent University, B-9000 Ghent, Belgium*

## Key words

$TiO_2$, thin film, photocatalysis, sol-gel, dip-coating, kinetics

## Abstract

$TiO_2$ thin films have been produced by a dip-coating process using a non-aqueous sol-gel method. This study investigated the influence of the operating variables such as nature of the substrate, sol concentration, withdrawing speed of the dip-coater and number of layers on the physico-chemical properties of the films using XRD, GIXRD, UV-Vis spectroscopy, profilometry, spectroscopic ellipsometry and SEM. Photocatalytic activity of the films was

* Corresponding author. Tel. : +32 4366 3540 ; fax : +32 4366 3545.
E-mail address : charline.malengreaux@ulg.ac.be (C.M. Malengreaux)

evaluated by following the degradation of methylene blue under artificial UV light at 25°C. The performances of the catalysts were compared through the reaction rate constants determined using an apparent first-order kinetic model adjusted on the experimental data. This study showed that the photocatalytic activity and the reaction rate constant depend on the film thickness through the synthesis and dipping variable, with an optimum thickness of 80 nm being observed. An optimized transparent film exhibiting a high adhesion, a well crystallized $TiO_2$-anatase phase, a good photocatalytic activity and a reaction rate constant $k$ equal to 0.126 $h^{-1}$ was obtained using a simple process. The specific photocatalytic activity of this film was higher to the one measured for $TiO_2$ powders in previous works.

# 1 Introduction

Environmental pollution has become a critical issue for our society and numerous studies based on heterogeneous semiconductor photocatalysis have been carried out in order to develop materials allowing air and water purification by using natural or artificial light illumination [1, 2]. The most frequently used photocatalyst is titanium oxide, $TiO_2$, due to its high oxidative potential, chemical stability, availability and its relatively low price [3, 4]. Electron-hole pairs are generated when $TiO_2$ is illuminated with UV light. The electrons and holes respectively reduce and oxidize the pollutant adsorbed on the photocatalyst surface by producing radical species such as $^{\cdot}OH$ radicals and $O_2^{\cdot -}$ superoxides [2-5].

In recent decades, the sol-gel method has become an interesting approach for the synthesis of $TiO_2$ bulk [6-9], thin films [10, 11] or hybrid membrane [12]. Homogeneous and highly pure thin films with controlled thickness, composition and microstructure can be prepared by different processes such as dip-coating, spin-coating or spray-coating from a liquid sol-gel solution. Dip-coating is a simple process where the substrate is immersed in a liquid and then withdrawn at a well-defined speed under controlled temperature and atmospheric conditions [13-15].

When precursors such as titanium alkoxides are used, the hydrolysis and condensation reactions are so exothermic and violent that they often lead to formation of a white precipitate by reaction with water or even the atmospheric humidity [16, 17]. To prevent precipitation, complexing ligands (e.g. $\beta$-diketones or carboxylic acids) can be used to modify the reactivity of the titanium alkoxide by increasing the coordination number of the metal and decreasing the number of hydrolysable groups. By using such modified precursors and a

substoichiometric amount of water, which means that the hydrolysis ratio ($H = n_{H2O}/n_{TTIP}$) is lower than 1, the hydrolysis and condensation sequence can be completely controlled [18-20].

A perfect control of the hydrolysis and condensation reactions of the titanium alkoxides also leads to a better control of the $TiO_2$ particle size [21].

Different non-aqueous synthetic routes to obtain the Ti-O-Ti network have been studied using different titanium alkoxides precursors complexed by acetylacetone and an in situ production of water through an esterification reaction initiated by the addition of acetic acid in the system [15, 22, 23].

In the last decade, the photocatalytic degradation of methylene blue under artificial UV light in the presence of $TiO_2$ based catalyst has been widely used as a reference test to assess the photocatalytic activity of a catalyst [11, 23]. It is generally admitted that a Langmuir-Hinshelwood (L-H) expression can be used to describe the photocatalytic discoloration of dye. In the cases where the initial dye concentration is a millimolar solution, the L-H equation can be simplified to an apparent first-order equation [24]. Several examples of dye degradation using $TiO_2$ powders as catalyst and adhering to this process have been reported [9, 11, 25, 26]. In those studies, it has been shown that the dye interacts strongly with the catalyst and then, the time required to reach the adsorption equilibrium is relatively long. In order to evaluate the actual degradation of the dye due to the catalyst it is required to replace the impoverished dye solution by a fresh dye solution after adsorption in the dark.

A previous study performed in our laboratory [9] reported that the degradation of methylene blue under artificial UV light using different $TiO_2$ powders prepared by sol-gel processing can be described using an apparent first-order equation. In this case the values obtained for the apparent reaction rate constant vary from 0.072 $h^{-1}$ to 0.234 $h^{-1}$ for a series of photocatalysts according to various thermal treatments performed. Another study reported in the literature

[27] showed that the photocatalytic activity of films produced by a spray pyrolysis method can also be described using an apparent first-order equation and in this case, the value of apparent reaction rate constant vary from 0.017 $h^{-1}$ to 0.037 $h^{-1}$.

Different reviews [28, 29] reported that the direct comparison of the behaviour of various catalysts is extremely difficult due to the different methods of preparation employed which lead to the production of powder, films or single crystals that are dramatically different in terms of concentration, crystalline type and surface area. So, it is important to remember that quantitative comparison of the activity of catalysts produced with different methods is justify only in the case where the activity of the different catalysts is evaluated by using the same experimental procedure (nature and concentration of the pollutant, type of illumination and distance catalyst-light source).

In this study, $TiO_2$ sols were prepared by a non-aqueous sol-gel method involving (i) the complexation of the titanium alkoxide precursor and (ii) an in situ production of water. Different stable sols were obtained and used to produce dip-coated films. Substrates were dipped one, two and three times with four different withdrawing speeds in order to investigate the effect of the precursor concentration, withdrawing speed and number of dippings on the film properties. The physico-chemical properties of the films were characterized by XRD, GIXRD, UV-Vis spectroscopy, profilometry, spectroscopic ellipsometry and SEM. The photocatalytic activity of the films was evaluated by following the degradation of methylene blue under artificial UV light. An apparent first-order kinetic model adjusted on the experimental data was used to determine the reaction rate constant for each film and to facilitate the comparison of the photocatalytic performances. The aim of this paper is to relate photocatalytic activity with synthesis operating variables through a detailed physico-chemical characterization and to show that beyond an optimal thickness the properties, the activity as

well as the reaction rate constant of the films reached optimum values. The study also showed that a simple process can be employed to produce thin films presenting specific photocatalytic activity comparable to the one measured for films produced with a spray pyrolysis method and higher than the one measured for $TiO_2$ powder.

# 2 Experimental

## 2.1 Preparation of $TiO_2$ sols

Different stable $TiO_2$ sols were prepared following the synthesis proposed by Legrand-Buscema et al. [15]. First titanium tetraisopropoxyde (TTIP > 98%, CAS 546-68-9, Merck) was dissolved in dry isopropanol (IPA, CAS 67-63-0, Thermofisher) and vigorously stirred at room temperature for 30 min. The syntheses were performed at room temperature under a constant nitrogen flow in order to avoid the precipitation of the TTIP by reaction with the air humidity when the atmosphere is uncontrolled. Pure acetylacetone (AcAc, CAS 123-54-6, Thermofisher) was added with a molar ratio [AcAc]/[TTIP] equal to 0.3 and the mixture was stirred for 1 h. Finally glacial acetic acid (HAc, CAS 64-19-7, Thermofisher) was slowly added into the solution to initialize the hydrolysis via an esterification reaction which leads to the in situ production of water. The molar ratio [HAc/[TTIP] was equal to 0.2. Sols with different TTIP concentrations (0.1, 0.3 and 0.5 mol $L^{-1}$) were synthesized. Transparent yellow solutions were obtained and they remained liquid for more than 6 months.

## 2.2 Characterization of sols

The viscosity of sols was measured using a LVDVII-Pro viscosimeter (Brookfield) equipped with a cup which allows the atmosphere and the temperature of the sample to be controlled. Viscosity values were measured every two days over a period of two weeks under a constant nitrogen flow ($0.1 \times 10^{-3}$ mol $min^{-1}$) and at 27°C. The measurements obtained were quite reproducible and the average viscosity was $1.67 \times 10^{-3}$, $1.74 \times 10^{-3}$ and $1.9 \times 10^{-3}$ Pa s respectively for sols with TTIP concentrations of 0.1, 0.3 and 0.5 mol $L^{-1}$.

### 2.3 Preparation of $TiO_2$ thin films

Single layer and multilayer $TiO_2$ thin films were prepared (Fig. 1) by dip-coating (Dip-Coater KSV-DC, KSV Instrument) using different dipping and withdrawing speeds (10, 30, 60 and 90 mm $min^{-1}$) on two different substrates: soda-lime glass (Marienfield Superior – 25 mm × 75 mm × 1 mm) and alkaline free glass (Schott Glass AF37, alkaline-earth aluminosilicate glass, alkali- and arsenic free in synthesis – 25 mm × 75 mm × 0.7 mm). After withdrawing, the films were dried at room temperature for 5 h and then calcined in air at 500°C for 1 h using a heating rate of 10°C $min^{-1}$ in order to maximize the photocatalytic activity of the films [30]. Then the films were cooled down to room temperature at a similar cooling rate. For the multilayer films the heat treatment was conducted between each dipping/withdrawing cycle into the precursor solution. A coating cycle is then defined as the process from the dipping/withdrawing steps to the calcination step at 500°C (Fig.1) and the final substrates have a $TiO_2$ covered surface of $12.5 \times 10^{-4}$ $m^2$.

### 2.4 Powder characterization

$TiO_2$ powders, synthesized from the same precursors as the thin films, were characterized using several techniques. 20 mL of each sol was dried in a Petri dish at room temperature in order to obtain a gel. The gels were then calcined with the same thermal treatment as the corresponding films. The crystallographic properties of the resulting $TiO_2$ powders were studied through the X-Ray Diffraction (XRD) patterns recorded with a Siemens D5000 powder diffractometer using Cu-Kα radiation, a Ni filter and operating conditions of 40 kV and 40 mA. The size of the $TiO_2$ crystallites, *d*, was estimated from XRD peak broadening by the Scherrer method:

$$d = 0.9\frac{\lambda}{(B\cos(\theta))} \qquad \text{(Eq. 1)}$$

with $B$ the full-width at half maximum after correction of the instrumental broadening, $\lambda$ the wavelength (nm) and $\theta$ the Bragg angle (rad) [31].

The optical properties were evaluated by performing Diffuse Reflectance Spectroscopy measurements (DR-UV-Vis) in the region 250 – 800 nm with a Varian Cary 5000 UV-Vis-NIR spectrophotometer, equipped with an integrating sphere (Varian External DRA-2500) and using $BaSO_4$ as reference. The UV-Vis spectra recorded in diffuse reflectance ($R_{sample}$) mode were transformed by using the Kubelka–Munk function:

$$F(R_\infty) = \frac{(1-R_\infty)^2}{2R_\infty} \qquad \text{(Eq. 2)}$$

$R_\infty$ is defined as $R_\infty = R_{sample}/R_{reference}$ , where $R_{reference}$ is the reflectance measured for an uncoated alkaline free substrate [32, 33]. For the sake of comparison, all spectra were normalized in intensity to 1.0 by dividing each spectrum by its maximum [34].

Using the well-known equation:

$$(F(R_\infty)h\nu)^2 = C(h\nu - E_g) \quad \text{(Eq. 3)}$$

where $C$ is a constant, the direct optical band-gap values, $E_g$ (eV), were obtained by plotting $(F(R_\infty)h\nu)^2$ as a function of the photon energy $h\nu$ and by the intersection of the linear part of the curve and the x-axis [35].

The bulk densities were obtained from weight and volume measurements and skeletal densities were measured by helium pycnometry [36]. Nitrogen adsorption-desorption isotherms were measured at 77 K on a Fisons Sorptomatics 1990 after outgassing for 24 h at room temperature. Textural properties were calculated using a coherent set of well-known techniques [37].

## 2.5 Film characterization

The adhesion of the coating to the substrates was assessed by a scotch tape test (3M's scotch tape). Each coating was covered with a piece of scotch tape and the adherence was considered adequate if the removal of the tape did not cause visible damages to the coating [11].

Crystallographic properties of the $TiO_2$ films were investigated by using Grazing Incidence X-Ray Diffraction (GIXRD, Bruker D8). The diffractometer using the Cu-Kα radiation was operated at 40 kV and 40 mA with an incident beam angle of 0.3°. The size of $TiO_2$ crystallites was estimated from GIXRD peak broadening by the Scherrer method (Eq.1).

The thicknesses were measured using a surface profilometer (Veeco, Dektak 8 Stylus Profiler) for the single layer films. Cross section observations by scanning electron microscopy (SEM FEI Quanta 200 F) enabled the thickness of the multilayer film to be estimated. SEM samples were prepared according to the following procedure: films were cut into pieces (25 mm × 20 mm × 0.7 mm), immobilized in different epoxy-resin samples in a vertical orientation and then polished in order to allow SEM cross section observations.

Film thickness and refractive index were also determined by spectroscopic ellipsometry (SE, J.A. Woollam Co. Inc., M-2000FI). A Cody-Lorentz dispersion model including surface roughness of the $TiO_2$ films was used to fit the optical constants with the Complete Ease Software (Woollam Inc.) [22]. If the films are modelled as a mixture of $TiO_2$ with air, an estimation of the film porosity, i.e. the void fraction in the film $\varepsilon_F$, can be calculated using Eq. 4 and the measurements of the refractive index, as described by Eufinger at al. [38].

$$(1-\varepsilon_F) = \frac{(n^2-1)}{(n_i^2-1)} \cdot \frac{(n_i^2+2)}{(n^2+2)} \qquad \text{(Eq. 4)}$$

with $n_i$ the reference refractive index of bulk $TiO_2$-anatase ($n_i$ = 2.462), $n$ the refractive index measured at 632.8 nm.

Using the spectroscopic ellipsometry measurements, the light absorption coefficient $\alpha$ can also be calculated by:

$$\alpha = \frac{4\pi k}{\lambda} \qquad \text{(Eq. 5)}$$

where $\lambda$ is the wavelength (nm) and $k$ is the extinction coefficient corresponding to the imaginary part of the refractive index $n$. Using the well-known equation:

$$\alpha^2 = \alpha_0 (h\nu - E_g) \qquad \text{(Eq. 6)}$$

where $\alpha_0$ is a constant, the direct optical band-gap values, $E_g$ (eV), can be obtained by plotting $\alpha^2$ as a function of the photon energy $h\nu$ and by the intersection of the linear part of the curve and the x-axis [22].

### 2.6 Photocatalytic activity of the films

The photocatalytic activity of each $TiO_2$ thin film was evaluated by following the degradation of methylene blue (MB) which was used as a model molecule to represent a pollutant [11, 23]. The films were placed at the bottom of a plastic Petri dish and immersed in a solution of MB ($2 \times 10^{-5}$ mol $L^{-1}$) and the dishes were closed with a plastic lid in order to avoid evaporation. First of all the MB concentration was monitored for 24 h for uncoated substrates and the $TiO_2$ films kept in the dark. This test was performed in order to determine if the MB is adsorbed by the films or the substrates or whether there is any MB breakdown under dark conditions. After this dark test, the films were irradiated with a commercial UV ($\lambda$ = 365 nm) fluorescent lamp (Osram Sylvania, Blacklight-Bleu Lamp, F18W/BLB-T8) over a 24 h

period. For each tested film a blank reference measurement was also performed as follows: a second Petri dish containing an uncoated glass substrate immersed in the MB solution was placed under UV light next to the Petri dish containing the tested film. The spectrum of the lamp was measured with a photometer (Hamamatsu) and it was found that the light can be considered as monochromatic ($\lambda$ = 365 nm). The degradation of the MB was determined by measuring the absorbance of the solution every hour using a Genesys 10S UV-Vis spectrophotometer (Thermo Scientific) at $\lambda$ = 665 nm every hour [17]. For each photocatalytic test, the temperature was kept constant at 25°C.

# 3 Results

## 3.1 X-Ray Diffraction on powders

In Fig. 2 the XRD patterns of $TiO_2$ powders obtained after calcination of gels corresponding to the different TTIP concentrations show that, in all cases, the material is constituted of $TiO_2$-anatase and it was observed that XRD patterns are not influenced by the variation in TTIP concentration in the corresponding sol. No traces of $TiO_2$-rutile phase formation were found.

## 3.2 UV-Vis diffuse reflectance on powders

Fig. 3a shows the evolution of the normalized Kubelka–Munk function $F(R_\infty)$ with the wavelength, $\lambda$, for powders corresponding to the different TTIP concentrations. In all cases, an absorbance band maximum is observed at wavelengths around 350 nm. Fig. 3b presents the evolution of the transformed Kubelka–Munk function $(F(R_\infty)hv)^2$ with energy $hv$. For powder obtained from the 0.1 mol $L^{-1}$ sol, as an example, the intersection between the linear fit 1 and the energy axis yields the direct band gap value $E_g = 3.18$ eV. By using the same procedure the direct band gap values for powders obtained from 0.3 mol $L^{-1}$ and 0.5 mol $L^{-1}$ sols were $E_g = 3.09$ eV and $E_g = 3.10$ eV, respectively. Those band gaps are in good agreement with values reported in a previous study for the $TiO_2$-anatase phase.

## 3.3 Textural properties of powders

Table 1 summarizes the textural properties determined for the powders. The specific surface area, $S_{BET}$ , the total specific porous volume, $V_p$, which is the liquid volume adsorbed at saturation pressure of nitrogen and the microporous volume, $V_{micro}$, were determined using BET analysis and Dubinin-Raduskevich theory. In all cases, isotherms show a hysteresis at

$p/p_0$ between 0.4 and 0.8, due to capillary condensation in mesopores [37]. Hence the volume of mesopores, $V_{meso}$, can be calculated by the difference between $V_p$ and $V_{micro}$. Using the value of the skeletal density measured by helium pycnometry, the porosity, i.e. the void fraction of the powder, $\varepsilon_P$, can be estimated for each powder using:

$$\varepsilon_P = \frac{V_p}{(V_p + \frac{1}{\rho_s})} \qquad \text{(Eq. 7)}$$

where $V_p$ is the specific porous volume ($cm^3\ g^{-1}$) and $\rho_s$ is the apparent density ($g\ cm^{-3}$). The results establish that the specific surface area, $S_{BET,}$ decreases with increasing the concentration of TTIP in the sol while the density increases for sols more concentrated in TTIP. The mesoporous volume is almost the same for each powder and finally the void fraction in the powders after calcination is around 30% in all cases.

### 3.4 Macroscopic observations of films

Compositions of sol corresponding to a concentration of TTIP of 0.1, 0.3 or 0.5 mol $L^{-1}$ enabled the production of homogeneous and transparent films with a smooth aspect and uniformly coloured reflections due to light interference effects. The scotch tape tests performed showed the films were well adhered to the substrates.

### 3.5 Grazing Incidence X-Ray Diffraction of films

The effect of the number of dippings, precursor concentration and withdrawing speed on the crystallographic properties of the films were investigated. No reflections and especially no diffraction peaks corresponding to $TiO_2$-anatase were detected for films deposited on soda-lime (SL) glass substrates whatever the composition of the precursor solution, the dipping speed or number of dippings, even after calcination. In contrast, GIXRD patterns show

diffraction peaks corresponding only to $TiO_2$-anatase for the films deposited on alkaline free (AF) glass substrates after calcination at 500°C.

As an example the influence of the number of dippings, as well as the effect of the nature of the substrate, on GIXRD patterns is presented in Fig. 4 for films dipped one, two and three times in a precursor solution [TTIP] = 0.5 mol $L^{-1}$ using alkaline free substrate or soda-lime glass substrates and a withdrawing speed of 10 mm $min^{-1}$ and 90 mm $min^{-1}$.

On the first hand, no diffraction peaks were observed for films deposited on soda-lime glass substrate for 1, 2 or 3 layers films and for both withdrawing speeds (Fig. 4a and Fig. 4b). For films deposited on alkaline free glass substrate using a low withdrawing speed, it can be observed that the intensity of the peak increases with increasing the number of dipping cycles (Fig. 4a). On the other hand, if alkaline free glass substrate and a high withdrawing speed are used, the number of dippings does not influence the intensity of the peak, which reaches a maximum value after the first layer (Fig. 4b).

A comparison between Fig. 4a and Fig. 4b enables the influence of withdrawing speed on the intensity of the peak at constant precursor concentration and number of dippings to be investigated. The intensity of the peak increases when increasing the withdrawing speed for single and two-layer films. However, for three-layer films, it was observed that the GIXRD patterns are similar regardless of the withdrawing speed used. Similar observations about the increasing intensity of the peak with increasing withdrawing speed are made for films obtained by dipping one, two and three times in 0.1 and 0.3 mol $L^{-1}$ sols.

In order to study the influence of the precursor concentration, GIXRD patterns for films obtained by using sols corresponding to [TTIP] = 0.1 – 0.3 – 0.5 mol $L^{-1}$ using alkaline free glass and a speed of 90 mm $min^{-1}$ were analysed, as presented in Fig. 5 for one and three coating cycles. As expected, the intensity of the peak increases with the precursor

concentration as well as with the number of deposited layers excepted for patterns (b2) and (b3) which are essentially identical and reaches the same maximal intensity value as in Fig. 4b. Similar results are observed for the different withdrawing speeds.

In summary, by analyzing GIXRD patterns of each film produced, it has been shown that intensity of the peak detected increased with increasing number of dipping cycles, the concentration of sol and the withdrawing speed. It was also observed that the GIXRD patterns are no longer influenced by the deposition operating variables when the films are dipped three times in a sol corresponding to [TTIP] $\geq$ 0.3 mol $L^{-1}$ and with a withdrawing speed $\geq$ 60 mm $min^{-1}$.

These observations can be explained by the fact that the intensity of the GIXRD peaks is related to both the amount of crystalline material and the film thickness. Using GIXRD, the penetration depth of the X-rays into the films is really low and always the same if the angle is constant. By increasing the number of dippings and the withdrawing speed, the film thickness increases (see sections 3.6 and 3.7). In this case, the volume of $TiO_2$ probed by the X-rays increases and a larger number of crystallites are detectable, leading to more intense diffraction peaks. Beyond a certain point, the intensity of the peak reaches a maximum value and becomes independent of the operating variables, thus of film thickness, because the entire thickness of the film is not probed by the X-rays.

### 3.6 Profilometry and SEM microscopy

The thickness of the films deposited on alkaline free glass was measured by profilometry for single layer films and by cross section SEM micrographs for multilayer films. Table 2 shows the influence of the number of dippings, precursor concentration and withdrawing speed on the film thickness.

It has been evidenced that thickness increases with increasing sol concentration of TTIP and withdrawing speed and that it is possible to obtain the same thicknesses with different combinations of operating variables. The thickness estimated by SEM observations for multilayer films are well correlated with the profilometry results obtained for single layer films. The thickness of a three layers film can be estimated by multiplying the value measured for a single layer film obtained with the same combination of operating variables by the number of dipping cycles.

The good quality of the films (absence of cracks, good adhesion on the substrate, homogeneity of the layer, ect) can also be observed via SEM. As an example the SEM pictures obtained for films dipped three times at different withdrawing speeds in the sol corresponding to 0.5 mol $L^{-1}$ are presented in Fig. 6.

It has been observed that the coloration phenomenon observed on the films is strongly dependent on the thickness and vary from brown to yellow, blue and pink when the thickness increases. Films produced under the same conditions always exhibit the same interference colour, due to their comparable thickness.

### 3.7 Spectroscopic ellipsometry

Film thicknesses measured by spectroscopic ellipsometry analysis are presented in Table 2 for films deposited on alkaline free glass and in Table 3 for films deposited on soda-lime glass. The Cody-Lorentz optical model used in the software included surface roughness of the films as a parameter and the roughness values were found to be below 4.6 nm in all cases. The thicknesses determined by the fitting are in good agreement with the results obtained by profilometry and SEM observations and are more reproducible (measurement error ± 0.2 nm while ± 5 nm for profilometry measurements). By comparing the results in Tables 2 and 3, it can be observed that the thickness of the films evolves in the same proportions with

increasing sol concentration in TTIP and withdrawing speed but films deposited on soda-lime glass are thicker.

As an example, Fig. 7a shows the experimental and fitted results for the ellipsometric angles Ψ and Δ as functions of wavelength for a film dipped three times in a precursor solution with [TTIP] = 0.5 mol $L^{-1}$ using alkaline-free substrate and a withdrawing speed of 10 mm $min^{-1}$. It can be seen that the experimental data are very well fitted by the model. By using the value of the optical constant *k*, the absorption coefficient $\alpha$ was calculated between 250 and 1700 nm. Fig. 7b shows the evolution of the square of the absorption coefficient $\alpha^2$ with the energy ($h\nu$). The intersection between the linear fit and the energy axis gives the value of the direct band gap $E_g$ = 3.71 eV for the film.

Table 2 and Table 3 present the value of the direct band-gap calculated for the different films. No significant effect of the TTIP concentration in the sols, withdrawing speed or number of layers on the band gap value is observed. The measurements obtained are reproducible and the average direct band gap values is 3.75 ± 0.03 eV for films deposited on alkaline free glass and 4.00 ± 0.03 eV for films deposited on soda-lime glass.

The porosity of the films was also estimated from the spectroscopic ellipsometry results. The porosity was evaluated at three different moments (before the test in the dark, after the test in the dark and after the photocatalytic test under UV light) for 3-layer films deposited on both substrates. The data in table 4 show that the porosity of the films deposited on soda-lime glass is twice as high as the porosity of the films deposited on alkaline-free glass before the test in the dark. After immersion in the MB solution for 24 h it can be seen that the porosity of the films deposited on soda-lime glass decreases significantly while the porosity of the films deposited on alkaline free glass remains constant. The results also show that the porosity remains the same after the photocatalytic tests under UV light for 24 h for both substrates.

### 3.8 Photocatalytic activity of the films

After the test in the dark it was found that the MB concentrations in solution remain constant for both uncoated substrates if there is no illumination. For films coated on soda-lime substrate a blue coloration of the film was observed while a similar film coated on alkaline free substrate remains perfectly transparent after immersion for24 h in the MB solution in the dark. The absence of MB adsorption for the films coated on alkaline free substrate is a remarkable result which is rarely reported in the literature. The MB did not interact with the catalyst in the dark which means that it is not required to wait before turning on the illumination in order to reach the adsorption equilibrium. And it is not either required to replace the impoverished dye solution by a fresh dye solution after adsorption in the dark in order to measure the actual degradation of the dye. By following the dye concentration in the blank measurements, it has been observed that the UV illumination did not degrade the MB spontaneously in the absence of $TiO_2$. According to those results it has been concluded that the measured degradation of MB under UV illumination with $\lambda$ = 365 nm is only due to the presence of the catalyst. No significant activity was measured for films deposited on soda-lime glass. In contrast, Fig. 8 shows the percentage of MB degradation under UV light illumination during 24 h for 3-layer films on alkaline free glass using a withdrawing speed of 10, 30, 60 or 90 mm $min^{-1}$ respectively. As expected, the photocatalytic activity generally increases when increasing the TTIP concentration in the precursor sol. By comparing the figures corresponding to the different speeds, it can be evidenced that using a low withdrawing speed (10 mm $min^{-1}$), film exhibited higher photocatalytic activities with increasing precursor concentrations as illustrated in Fig. 8a, whereas for films dipped at higher speeds (30, 60 and 90 mm $min^{-1}$), it can be observed in Fig. 8b, c and d that the photocatalytic activity seemed to be essentially independent of the precursor concentration for [TTIP] $\geq$ 0.3 mol $L^{-1}$.

The measurements were repeated in order to demonstrate the reproducibility of the method. The results are quite similar to those displayed in Fig. 8 and the standard deviation $\sigma$ is 5% in all cases.

# 4 Discussion

By comparing the theoretical and experimental values of the mass of powders obtained after calcination at 500°C for 1 h, it has been evidenced that there is no loss of titanium dioxide suggesting a complete polymerisation of the alkoxide in agreement with a previous study.

The stability of the sols can be explained by the small amount of water produced in situ during the synthesis. The maximum hydrolysis ratio ($H = n_{H2O}/n_{TTIP}$) can be estimated to be equal to 0.2 considering a theoretical complete conversion of the acetic acid to the corresponding ester through the esterification reaction. $H = 0.2$ corresponds to a substoichiometric amounts of water and the TTIP is complexed by AcAc in order to decrease the number of hydrolysable groups. These synthesis conditions lead to the formation of a weakly-branched gel structure in the sol which is preferable to obtain homogeneous and crack-free films [13, 18, 22].

This study has revealed a significant effect of the substrate on the crystallographic properties of the film as well as on the photocatalytic activity. After calcination at 500°C, it appears that films on soda-lime glass are still amorphous whereas identical films deposited on alkaline free substrate as well as the corresponding powders are only constituted of the $TiO_2$-anatase phase as revealed by GIXRD. The direct band gap is higher for films deposited on soda-lime glass and the porosity of the films was also affected by the substrate. The films deposited on soda-lime glass do not exhibit any photocatalytic activity under the chosen UV light.

These effects of the soda-lime glass substrate can be explained by the migration of sodium ions from the substrate into the film during the heat treatment at 500°C. It has been reported in the literature that the sodium diffusion into the $TiO_2$ thin film is detrimental to the photocatalytic activity [14, 39-41]. It was suggested that high concentration of $Na^+$ inhibits

the crystallization of the photoactive $TiO_2$-anatase phase by decreasing the degree of crystallinity and by increasing the temperature needed for the crystallization, while $Na^+$ acts as a recombination centre for photogenerated electron-holes pairs even for low concentration of $Na^+$. A solution already proposed in the literature is to use a $SiO_2$ barrier layer between the substrate and the $TiO_2$ film in order to prevent the negative effect of the $Na^+$ diffusion in the photocatalyst [41, 42]. By using alkaline free glass as substrates instead of soda-lime glass covered with a primary barrier layer, a transparent $TiO_2$-anatase thin film photocatalyst with a good crystallization and thus a good activity can be obtained using less resources.

It is well known in the literature that the thickness of films produced by dip-coating mainly depends on the viscosity of the dipping solution and the withdrawing speed of the substrate [13]. It this study, it has been established that the viscosity of the precursor solutions increased with increasing TTIP concentration, leading to thicker films in agreement with results reported by Legrand-Buscema et al. [15]. It was also shown that increasing the withdrawing speed leads to thicker films even if the same sol is used, as expected. It is important to note that the influence of the precursor concentration is more important than the influence of the withdrawing speed on the film thickness. For multilayer films the SEM and spectroscopic ellipsometry observations showed that several coatings increase the thickness but do not affect the homogeneity and adhesion of the films and an estimation of the thickness of the multilayer films can be obtained simply by multiplying the thickness of the corresponding single layer films.

The $TiO_2$ particle size calculated by Eq. 1 both for powders and the corresponding films is around 18 nm and is not influenced by the synthesis and dip-coating variables such as precursor concentration, the withdrawing speed and number of cycles. This value has been

reported in previous studies as an appropriate size for good photocatalytic activity [17, 23, 43].

By comparing the GIXRD results and the measured thicknesses, it is possible to determine an optimum thickness corresponding to ~80 nm beyond which the synthesis and deposition variables no longer influence the film properties. For film thinner than 80 nm, more distinct GIXRD peaks with higher intensity are observed with increasing withdrawing speed and TTIP concentration suggesting that the material crystallinity is enhanced when the thickness increases [17, 23]. For films thicker than 80 nm, the GIXRD patterns are superimposable suggesting that the X-rays penetrate a certain thickness of the film which always presents the same degree of crystallinity independently of the dipping variables. It has been reported that a higher degree of crystallinity leads to a lower number of crystal defects and thus a limitation of the electron holes recombination which enhances the photocatalytic activity [38].

In order to compare the photocatalytic performances of the films, the activity of the films was defined as the percentage of MB degradation reached after 24 h under UV illumination and those values were plotted as a function of the film thickness (Fig. 9). It is evident that the activity of the catalyst depends on the film thickness through the synthesis and dipping variables as long as the same optimum thickness of 80 nm is not reached as it is presented in Fig. 9. In this case, the amount of catalyst involved in the photocatalytic reaction as well as the degree of crystallization increase when the thickness of the film increases leading to more active photocatalysts [10, 43, 44]. Another way to compare the performances of the different photocatalysts is to determine the reaction rate constant $k$ ($h^{-1}$) for each film. Different kinetic models were tested and it has been shown that the apparent first-order kinetic model fitted perfectly the experimental data:

$$\frac{C}{C_0} = \exp(-kt) \qquad \text{(Eq. 8)}$$

where $C$ is the concentration of dye (mol $L^{-1}$) at the illumination time $t$ (h) and $C_0$ is the initial concentration of dye (mol $L^{-1}$). As a function of the conversion $f$, equation (Eq. 8) becomes:

$$f = 1 - (\exp(-kt)) \qquad \text{(Eq. 9)}$$

For example, Fig. 10 shows the evolution of the conversion in MB as a function of the illumination time for a 3-layer films deposited on alkaline free glass using a sol corresponding to [TTIP] = 0.3 mol $L^{-1}$ and a withdrawing speed of 60 mm $min^{-1}$. The apparent first-order kinetic model shows a good correlation with the experimental data and the reaction rate constant $k$ is equal to 0.126 $h^{-1}$. The same model has been applied for each 3-layer film deposited on alkaline free glass. Fig. 11 presents the evolution of the different reaction rate constant $k$ as a function of the film thickness. It is clearly seen that the trend is exactly the same than in Fig. 9. Indeed the reaction rate constant also increased with the thickness of the films as long as the same optimum thickness of 80 nm is not reached.

In order to compare quantitatively the activity of films, the apparent reaction rate per surface unit $k_s$ ($h^{-1}m^{-2}$) has been used to determine the specific activity of each catalyst. In our case, this value of $k_s$ is equal to 90 $h^{-1}m^{-2}$ while the value of $k_s$ reported by Lopez et al. [27] for films produced with a spray pyrolysis method is equal to 93 $h^{-1}m^{-2}$. These values are of the same order of magnitude which means that the deposition method does not influence the specific activity of these films.

In the case of a quantitatively comparison of the activity of films and powders, the optimum value of $k$ presented by Paez et al. [9] for a $TiO_2$-anatase powder obtained by a sol-gel process and treated at 500°C is equal to 0.126 $h^{-1}$. In a typical experiment, the catalyst concentration

of in the MB solution was 1 g $L^{-1}$ with a reaction volume of 0.05 L and the specific surface area of the catalyst was 5 $m^2$ $g^{-1}$. In this case, the value of the apparent reaction rate per surface unit is much lower for the powder than for our film and we can conclude than the specific activity of the film is higher.

The results obtained established that, beyond the optimum thickness, the detected crystallinity, the measured activity and the apparent reaction rate are similar for the different films, independent of the total amount of $TiO_2$ deposited on the substrate. The following factors are suggested to explain this limitation. First the internal diffusion of the pollutant and the charge carriers through the photocatalyst film are limited meaning that only the accessible part of the film is involved in the photocatalytic reaction. Secondly the possible aggregation and growth of $TiO_2$ crystallites in the interior region of thick films, which underwent three heat-treatment cycles, can cause a decrease in the number of active sites. Finally, the increasing opacity of the thick films can lead to a decrease in the UV light transmission through the films. In the present case, the films produced are relatively thin, thus the transmission of the UV light remains high and the amount of absorbed light can be considered to be proportional to the film thickness. These hypotheses have been reported in the literature [38, 44, 45].

Considering that only the upper part of the film is involved in the photocatalytic reaction and according to the GIXRD results showing that the degree of crystallinity is similar for films thicker than 80 nm, it seems quite logical that the activity measured for those films leads to the same percentage of degradation after 24 h. The values of the reaction rate constant are also similar for films thicker than 80 nm. In this case, it can be suggested that it is unnecessary to produce films thicker than 80 nm for this type of pollutant degraded by this specific installation.

# 5 Conclusions

This study showed that it was possible to produce transparent, adherent, homogeneous and photocatalyticaly active $TiO_2$ thin films with thickness between 20 and 250 nm by dip-coating on a glass substrate using a sol-gel method. These films present a specific photocatalytic activity higher to the one measured for $TiO_2$ powder in previous works.

A non-aqueous sol-gel method using titanium tetraisopropoxide, isopropanol, acetylacetone and acetic acid was used to synthesize different stable sols by controlling the hydrolysis reaction of the titanium alkoxide. Those sols were used to produce transparent $TiO_2$ thin films on soda-lime glass and alkaline free glass by dip-coating. The effect of the substrate was investigated and it has been evidenced that films deposited on alkaline free glass exhibit a well crystallized $TiO_2$-anatase phase, a lower porosity, a lower direct band gap and a good photocatalytic activity under UV light whereas films deposited on soda-lime glass were amorphous, more porous and inactive.

The influence of the precursor concentration and operating variables was also studied and the results showed that crystallinity and photoactivity were mainly correlated to the film thickness. Thickness can be increased by increasing the withdrawing speed, the TTIP concentration in the sol or the number of dipping cycles. It has been shown that the film thicknesses reached after multiple depositions can be estimated by multiplying the measured value of the corresponding single layer films.

The experiment of photocatalytic degradation of MB established that an increasing in the film thickness improved the photocatalytic activity of the films as long as the optimum value of ~ 80 nm was not reached. An apparent first-order kinetic model was used to determine the reaction rate constant for each film and to facilitate the comparison of the photocatalytic

performances. The same tendency has been observed for the influence of the film thickness on the apparent reaction rate value; beyond the optimum value of ~ 80 nm, the apparent reaction rate constant reaches an optimum value whatever the thickness of the films.

Beyond that limit the properties of the films, the photocatalytic activity as well as the apparent reaction rate constant were not influenced anymore by the deposition variables. An optimized transparent film exhibiting a high adhesion, a well crystallized $TiO_2$-anatase phase and an interesting photocatalytic activity for the aqueous degradation of MB under UV light was obtained by dipping three times an alkaline free glass substrate in a sol with [TTIP] = 0.3 mol $L^{-1}$ using a withdrawing speed of 60 or 90 mm $min^{-1}$ and a heat treatment of 1 h at 500°C between each dipping. After 24 h of illumination, 93% of the MB was degraded and the value of the apparent reaction rate constant *k* was equal to 0.126 $h^{-1}$.

# 6 Acknowledgments

C.M. Malengreaux, S.L. Pirard and S.D. Lambert are grateful to the F.R.S.– FNRS for PhD grant, postdoctoral researcher and research associate positions respectively. The authors are grateful to Mr. O. Janssens, Ghent University for performing the SEM measurements, to Dr. D. Wicky, ArcelorMittal Liège Research, for performing some profilometry measurements, to Pr. B. Vertruyen, University of Liège, for her helpful comments during the acquisition of GIXRD and XRD measurements, and to Dr. L. Tasseroul, University of Liège, for her advice for photocatalytic measurements. The authors also acknowledge the Interuniversity Attraction Pole (IAP-P6/17), the Ministère de la Région Wallonne, the Fonds de la Recherche Fondamentale Collective and the Fonds Wetenschappelijk Onderzoek Vlaanderen for their financial support.

# 7 References


[1] A. Fujishima, X. Zhang, D.A. Tryk, Heterogeneous photocatalysis: From water photolysis to applications in environmental cleanup, Int J Hydrog Energy, 32 (2007) 2664-2672.

[2] A. Nakajima, A. Nakamura, N. Arimitsu, Y. Kameshima, K. Okada, Processing and properties of transparent sulfated $TiO_2$ thin films using sol-gel method, Thin Solid Films, 516 (2008) 6392-6397.

[3] A. Mills, S. LeHunte, An overview of semiconductor photocatalysis, J Photochem Photobiol A-Chem, 108 (1997) 1-35.

[4] D.A. Tryk, A. Fujishima, K. Honda, Recent topics in photoelectrochemistry: achievements and future prospects, Electrochim Acta, 45 (2000) 2363-2376.

[5] A. Fujishima, K. Hashimoto, T. Watanabe, $TiO_2$ Photocatalysis: Fundamentals and Applications, in, BKC, Inc, Tokyo, 1999.

[6] A.J. Maira, K.L. Yeung, J. Soria, J.M. Coronado, C. Belver, C.Y. Lee, Gas-phase photo-oxidation of toluene using nanometer-size $TiO_2$ catalysts, Appl Catal B-Environ, 29 (2001) 327-336.

[7] B.L. Zhang, B.S. Chen, K.Y. Shi, S.J. He, X.D. Liu, Z.J. Du, K.L. Yang, Preparation and characterization of nanocrystal grain $TiO_2$ porous microspheres, Appl Catal B-Environ, 40 (2003) 253-258.

[8] C.J. Bodson, S.D. Lambert, C. Alié, X. Cattoen, J.P. Pirard, C. Bied, M.Wong Chi Man, B. Heinrichs, Effects of additives and solvents on the gel formation rate and on the texture of P- and Si-doped $TiO_2$ materials, Micropor Mesopor Mat, 134 (2010) 157-164.

[9] C.A. Paez, D. Poelman, J.P. Pirard, B. Heinrichs, Unpredictable photocatalytic ability of $H_2$-reduced rutile-$TiO_2$ xerogel in the degradation of dye-pollutants under UV and visible light irradiation, Appl Catal B-Environ, 94 (2010) 263-271.

[10] Y.J. Chen, E. Stathatos, D.D. Dionysiou, Microstructure characterization and photocatalytic activity of mesoporous $TiO_2$ films with ultrafine anatase nanocrystallites, Surf Coat Tech, 202 (2008) 1944-1950.

[11] P. Novotna, J. Zita, J. Krysa, V. Kalousek, J. Rathousky, Two-component transparent $TiO_2/SiO_2$ and $TiO_2$/PDMS films as efficient photocatalysts for environmental cleaning, Appl Catal B-Environ, 79 (2008) 179-185.

[12] A.J. Maira, W.N. Lau, C.Y. Lee, P.L. Yue, C.K. Chan, K.L. Yeung, Performance of a membrane-catalyst for photocatalytic oxidation of volatile organic compounds, Chem Eng Sci, 58 (2003) 959-962.

[13] S.G.W. Brinker C. Jeffrey., Sol-gel science: the physics and chemistry of sol-gel processing, in, Academic Press, Boston, 1990.

[14] J.G. Yu, X.J. Zhao, Effect of surface treatment on the photocatalytic activity and hydrophilic property of the sol-gel derived $TiO_2$ thin films, Mater Res Bull, 36 (2001) 97-107.

[15] C. Legrand-Buscema, C. Malibert, S. Bach, Elaboration and characterization of thin films of $TiO_2$ prepared by sol-gel process, Thin Solid Films, 418 (2002) 79-84.

[16] G. Arrachart, D.J. Cassidy, I. Karatchevtseva, G. Triani, Nanostructural Evolution of Titania-Based Materials Using Modified Titanium Precursors, J Am Ceram Soc, 92 (2009) 2109-2115.

[17] H. Choi, E. Stathatos, D.D. Dionysiou, Synthesis of nanocrystalline photocatalytic $TiO_2$ thin films and particles using sol-gel method modified with nonionic surfactants, Thin Solid Films, 510 (2006) 107-114.

[18] U. Schubert, Chemical modification of titanium alkoxides for sol-gel processing, J Mater Chem, 15 (2005) 3701-3715.

[19] I. Karatchevtseva, A. Heinemann, V. Hartley, R. Knott, Structure of Organic-Inorganic Nanohybrids Incorporating Titanium(IV) Oxoalkoxyacylate Nanoclusters: A SANS Study, J Phys Chem B, 112 (2008) 16478-16484.

[20] L. Rozes, N. Steunou, G. Fornasieri, C. Sanchez, Titanium-oxo clusters, versatile nanobuilding blocks for the design of advanced hybrid materials, Mon Chem, 137 (2006) 501-528.

[21] A.J. Maira, K.L. Yeung, C.Y. Lee, P.L. Yue, C.K. Chan, Size Effects in Gas-Phase Photo-oxidation of Trichloroethylene Using Nanometer-Sized $TiO_2$ Catalysts, J Catal, 192 (2000) 185-196.

[22] N. Avci, P.F. Smet, H. Poelman, N. Van de Velde, K. De Buysser, I. Van Driessche, D. Poelman, Characterization of $TiO_2$ powders and thin films prepared by non-aqueous sol-gel techniques, J Sol-Gel Sci Techn, 52 (2009) 424-431.

[23] C. Euvananont, C. Junin, K. Inpor, P. Limthongkul, C. Thanachayanont, $TiO_2$ optical coating layers for self-cleaning applications, Ceram Int, 34 (2008) 1067-1071.

[24] M.A. Rauf, S.S. Ashraf, Fundamental principles and application of heterogeneous photocatalytic degradation of dyes in solution, Chem Eng J, 151 (2009) 10-18.

[25] A. Houas, H. Lachheb, M. Ksibi, E. Elaloui, C. Guillard, J.-M. Herrmann, Photocatalytic degradation pathway of methylene blue in water, Appl Catal B-Environ, 31 (2001) 145-157.

[26] J. Huang, Y. Cao, Z. Liu, Z. Deng, W. Wang, Application of titanate nanoflowers for dye removal: A comparative study with titanate nanotubes and nanowires, Chem Eng J, article in press (2012).

[27] A. López, D. Acosta, A. I. Martínez, J. Santiago, Nanostructured low crystallized titanium dioxide thin films with good photocatalytic activity, Powder Technol, 202 111-117.

[28] A. Mills, An overview of the methylene blue ISO test for assessing the activities of photocatalytic films, Appl Catal B-Environ, article in press (2012).

[29] A. Di Paola, E. García-López, G. Marcì, L. Palmisano, A survey of photocatalytic materials for environmental remediation, J Haz Mater, 211–212 (2012) 3-29.

[30] J.G. Yu, X.J. Zhao, Q.N. Zhao, Photocatalytic activity of nanometer $TiO_2$ thin films prepared by the sol-gel method, Mater Chem Phys, 69 (2001) 25-29.

[31] A.L. Patterson, Phys Rev, (1939) 978.

[32]P. Kubelka, Ein Beitrag zur Optik der Farbanstriche, Z Tech Phys, 12 (1931) 593-601.

[33] P. Kubelka, New contributions to the optics of intensly light-scattering materials, J Opt Amer, 38 (1948) 448-457.

[34] B. Braconnier, C.A. Paez, S. Lambert, C. Alié, C. Henrist, D. Poelman, J.P. Pirard, R. Cloots, B. Heinrichs, Ag- and $SiO_2$-doped porous $TiO_2$ with enhanced thermal stability, Micropor Mesopor Mat, 122 (2009) 247-254.

[35] A.E.M. Morales, E. Sanchez, U. Pal, Use of diffuse reflectance spectroscopy for optical characterization of un-supported nanostructures, Rev Mex Fis S, 53 (2007) 18-22.

[36] C. Alié, N. Tcherkassova, F. Ferauche, S. Lambert, B. Heinrichs, R. Pirard, J.P. Pirard, Multigram scale synthesis and characterization of low-density silica xerogels, J Non-Cryst Solids, 352 (2006) 2763-2771.

[37] A.J. Lecloux, Catalysis: Science and Technology, in, Springer, Berlin, 1981.

[38] K. Eufinger, D. Poelman, H. Poelman, R. De Gryse and G.B. Marin, $TiO_2$ thin films for photocatalytic applications, in: S. Nam (Ed.) Thin solid films : process and applications Transworld Research Network, Kerala, India 2008, pp. 189-227.

[39] H. Tomaszewski, K. Eufinger, H. Poelman, D. Poelman, R. De Gryse, P.F. Smet, G.B. Marin, Effect of substrate sodium content on crystallization and photocatalytic activity of

$TiO_2$ films prepared by DC magnetron sputtering, Int J Photoenergy, Art. No. 95213 (2007) 5.

[40] Y. Paz, A. Heller, Photo-oxidatively self-cleaning transparent titanium dioxide films on soda lime glass: The deleterious effect of sodium contamination and its prevention, J Mater Res, 12 (1997) 2759-2766.

[41] J. Zita, J. Krysa, A. Mills, Correlation of oxidative and reductive dye bleaching on $TiO_2$ photocatalyst films, J Photochem Photobiol A-Chem, 203 (2009) 119-124.

[42] M. Addamo, V. Augugliaro, A. Di Paola, E. Garcia-Lopez, V. Loddo, G. Marci, L. Palmisano, Photocatalytic thin films of $TiO_2$ formed by a sol-gel process using titanium tetraisopropoxide as the precursor, Thin Solid Films, 516 (2008) 3802-3807.

[43] S.H. Oh, J.S. Kim, J.S. Chung, E.J. Kim, S.H. Hahn, Crystallization and photoactivity of $TiO_2$ films formed on soda lime glass by a sol-gel dip-coating process, Chem Eng Commun, 192 (2005) 327-335.

[44] J.G. Yu, X.J. Zhao, Q.N. Zhao, Effect of film thickness on the grain size and photocatalytic activity of the sol-gel derived nanometer $TiO_2$ thin films, J Mater Sci Lett, 19 (2000) 1015-1017.

[45] D. Zare-Hossein-abadi, A. Ershad-Langroudi, A. Rahimi, S. Afsar, Photo-Generated Activities of Nanocrystalline $TiO_2$ Thin Films, J Inorg Organomet Polym Materone , 20 (2010) 250-257.

# Table 1

| Sample | [TTIP] | $S_{BET}$ | $V_p$ | $V_{micro}$ | $V_{meso}$ | $\rho_s$ | $\varepsilon_p$ |
|---|---|---|---|---|---|---|---|
| | (mol $L^{-1}$) | ($m^2 g^{-1}$) | ($cm^3 g^{-1}$) | ($cm^3 g^{-1}$) | ($cm^3 g^{-1}$) | (g $cm^{-3}$) | (% of void) |
| Powder 1 | 0.1 | 65 | 0.15 | 0.02 | 0.12 | 3.54 | 30 |
| Powder 2 | 0.3 | 35 | 0.12 | 0.01 | 0.11 | 3.93 | 29 |
| Powder 3 | 0.5 | 30 | 0.13 | 0.01 | 0.12 | 3.94 | 32 |

**Table(s)**

# Table 2

| Sample | [TTIP] | Withdrawing speed | Thickness 1 Layer | | Band Gap 1 Layer | Thickness 2 Layers | | Band Gap 2 Layers | Thickness 3 Layers | | Band Gap 3 Layers |
|---|---|---|---|---|---|---|---|---|---|---|---|
| | (mol $L^{-1}$) | (mm $min^{-1}$) | (nm) | | (eV) | (nm) | | (eV) | (nm) | | (eV) |
| AF1 | 0.1 | 10 | < 20 [b] | 10 [d] | 3.82[e] | - [f] | - | - | 21 [c] | 20 [d] | 3.76[e] |
| AF2 | 0.1 | 30 | < 20 | 12 | 3.78 | - | - | - | 22 | 27 | 3.77 |
| AF3 | 0.1 | 60 | < 20 | 15 | 3.79 | - | - | - | 37 | 35 | 3.68 |
| AF4 | 0.1 | 90 | < 20 | 19 | 3.80 | - | - | - | 42 | 43 | 3.67 |
| AF5 | 0.3 | 10 | 18[a] | 17 | 3.74 | - | 38 [d] | 3.73[e] | 52 | 54 | 3.76 |
| AF6 | 0.3 | 30 | 24 | 28 | 3.78 | - | 58 | 3.79 | 82 | 87 | 3.77 |
| AF7 | 0.3 | 60 | 48 | 42 | 3.73 | 91 [a] | 90 | 3.72 | 128 | 117 | 3.72 |
| AF8 | 0.3 | 90 | 63 | 62 | 3.75 | - | 116 | 3.73 | 151 | 158 | 3.72 |
| AF9 | 0.5 | 10 | 24 | 24 | 3.75 | - | 62 | 3.72 | 60 | 69 | 3.74 |
| AF10 | 0.5 | 30 | 34 | 33 | 3.75 | - | 88 | 3.83 | 113 | 109 | 3.71 |
| AF11 | 0.5 | 60 | 82 | 83 | 3.77 | - | 117 | 3.72 | 185 | 185 | 3.70 |
| AF12 | 0.5 | 90 | 91 | 95 | 3.76 | - | 180 | 3.79 | 260 | 265 | 3.79 |

# Table 3

| Sample | [TTIP] ($mol.L^{-1}$) | Withdrawing speed ($mm.min^{-1}$) | Thickness 1 layer (nm) | Band Gap 1 Layer (eV) | Thickness 3 layers (nm) | Band Gap 3 Layers (eV) |
|---|---|---|---|---|---|---|
| SL1 | 0.1 | 10 | - [(a)] | - | 26 | 4.04 |
| SL2 | 0.1 | 30 | - | - | 35 | 4.00 |
| SL3 | 0.1 | 60 | - | - | 43 | 3.98 |
| SL4 | 0.1 | 90 | - | - | 50 | 3.98 |
| SL5 | 0.3 | 10 | - | - | 42 | 4.07 |
| SL6 | 0.3 | 30 | - | - | 83 | 4.00 |
| SL7 | 0.3 | 60 | - | - | 137 | 4.00 |
| SL8 | 0.3 | 90 | - | - | 179 | 3.98 |
| SL9 | 0.5 | 10 | 45 | 3.98 | 79 | 4.00 |
| SL10 | 0.5 | 30 | 46 | 4.03 | 125 | 3.95 |
| SL11 | 0.5 | 60 | 78 | 4.00 | 209 | 3.92 |
| SL12 | 0.5 | 90 | 93 | 4.01 | 278 | 3.97 |

# Table 4

| Sample 3 layers | Porosity Before DT | Porosity After DT (% of void) | Porosity After PCT | Sample 3 layers | Porosity Before DT | Porosity After DT (% of void) | Porosity After PCT |
|---|---|---|---|---|---|---|---|
| AF1 | 10 | 11 | 11 | SL1 | 20 | 8 | 7 |
| AF2 | 11 | 11 | 10 | SL2 | 20 | 5 | 5 |
| AF3 | 8 | 8 | 8 | SL3 | 20 | 7 | 8 |
| AF4 | 8 | 8 | 8 | SL4 | 18 | 9 | 10 |
| AF5 | 13 | 10 | 11 | SL5 | 20 | 6 | 6 |
| AF6 | 8 | 9 | 10 | SL6 | 21 | 7 | 6 |
| AF7 | 8 | 9 | 8 | SL7 | 23 | 9 | 8 |
| AF8 | 13 | 13 | 13 | SL8 | 23 | 8 | 7 |
| AF9 | 14 | 15 | 15 | SL9 | 20 | 9 | 8 |
| AF10 | 3 | 3 | 3 | SL10 | 14 | 7 | 5 |
| AF11 | 4 | 6 | 6 | SL11 | 18 | 6 | 7 |
| AF12 | 10 | 9 | 7 | SL12 | 19 | 8 | 7 |

# List of tables

Figure(s)

# Figure 1

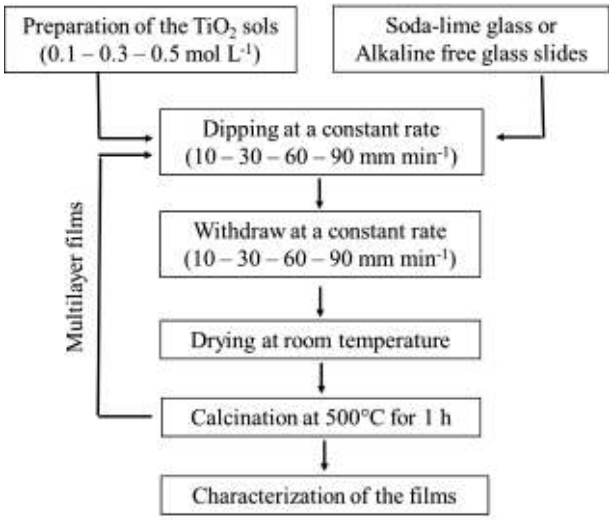

# Figure 2

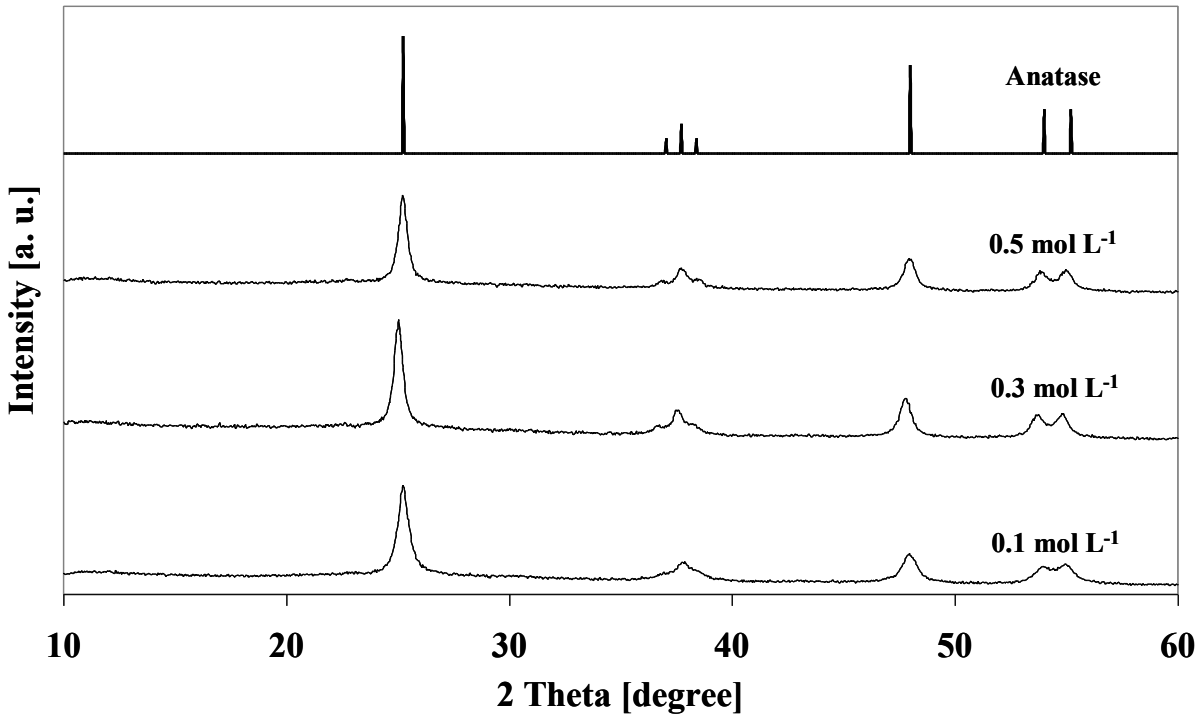
Anatase
0.5 mol L-1
0.3 mol L-1
0.1 mol L-1
Intensity [a. u.]
10
20
30
40
50
60
2 Theta [degree]

Figure(s)

# Figure 3

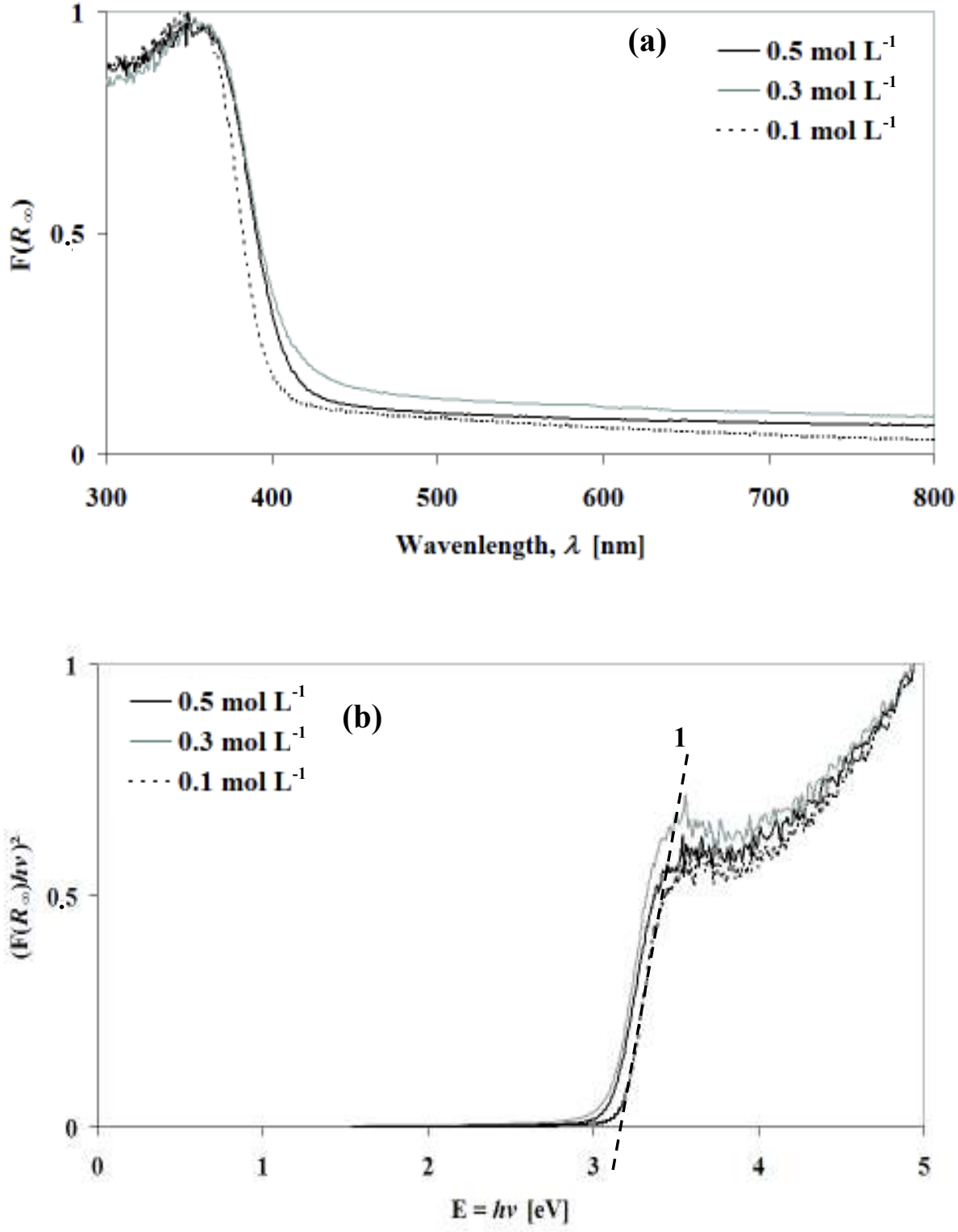

# Figure 4

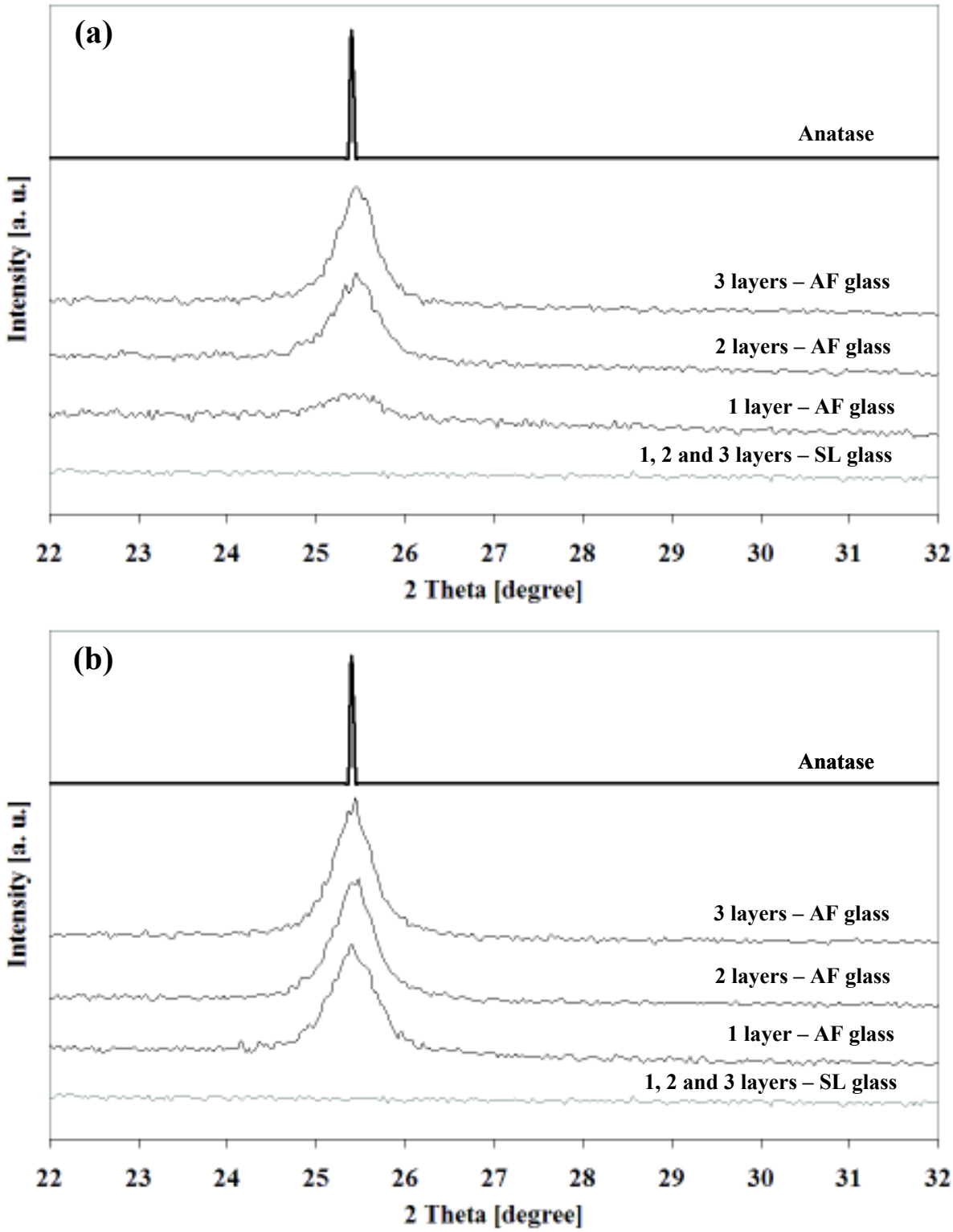
(a)
Anatase
3 layers – AF glass
2 layers – AF glass
1 layer – AF glass
1, 2 and 3 layers – SL glass
Intensity [a. u.]
22
23
24
25
26
27
28
29
30
31
32
2 Theta [degree]
(b)
Anatase
3 layers – AF glass
2 layers – AF glass
1 layer – AF glass
1, 2 and 3 layers – SL glass
Intensity [a. u.]
22
23
24
25
26
27
28
29
30
31
32
2 Theta [degree]

# Figure 5

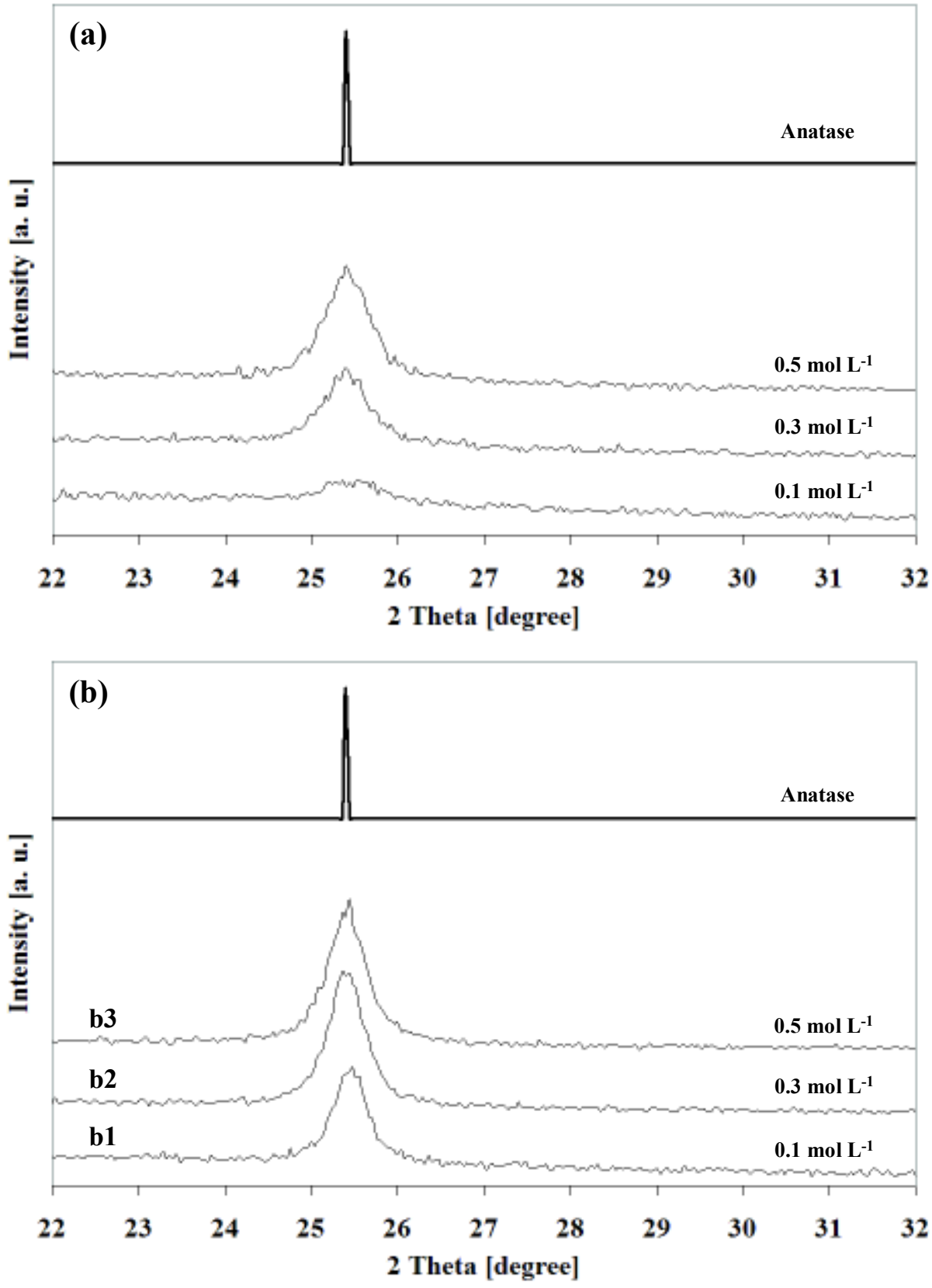
(a)
Anatase
Intensity [a. u.]
0.5 mol L-1
0.3 mol L-1
0.1 mol L-1
22
23
24
25
26
27
28
29
30
31
32
2 Theta [degree]
(b)
Anatase
Intensity [a. u.]
b3
b2
b1
0.5 mol L-1
0.3 mol L-1
0.1 mol L-1
22
23
24
25
26
27
28
29
30
31
32
2 Theta [degree]

## Figure 6

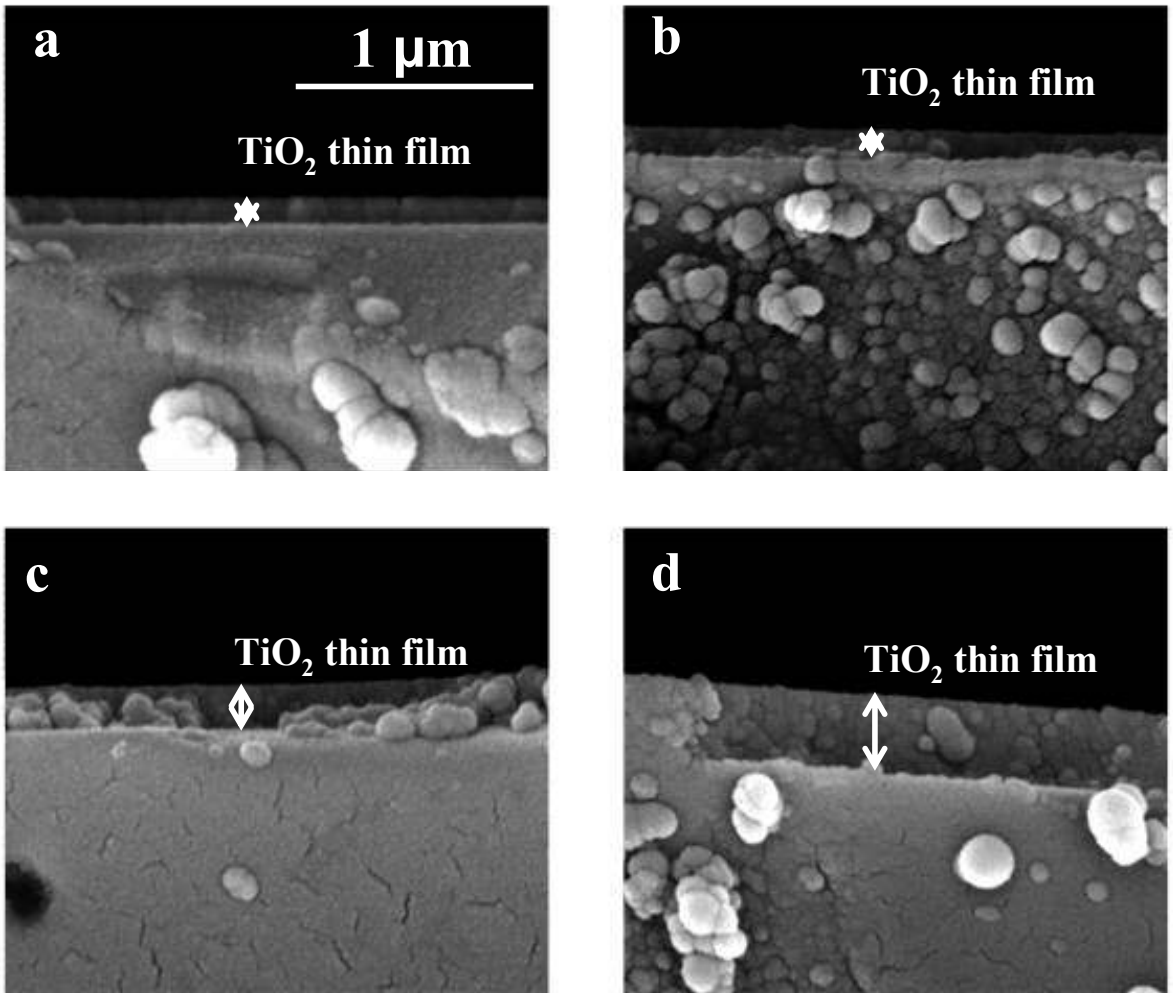
a
1 μm
TiO2 thin film
b
TiO2 thin film
c
TiO2 thin film
d
TiO2 thin film

Figure(s)

# Figure 7

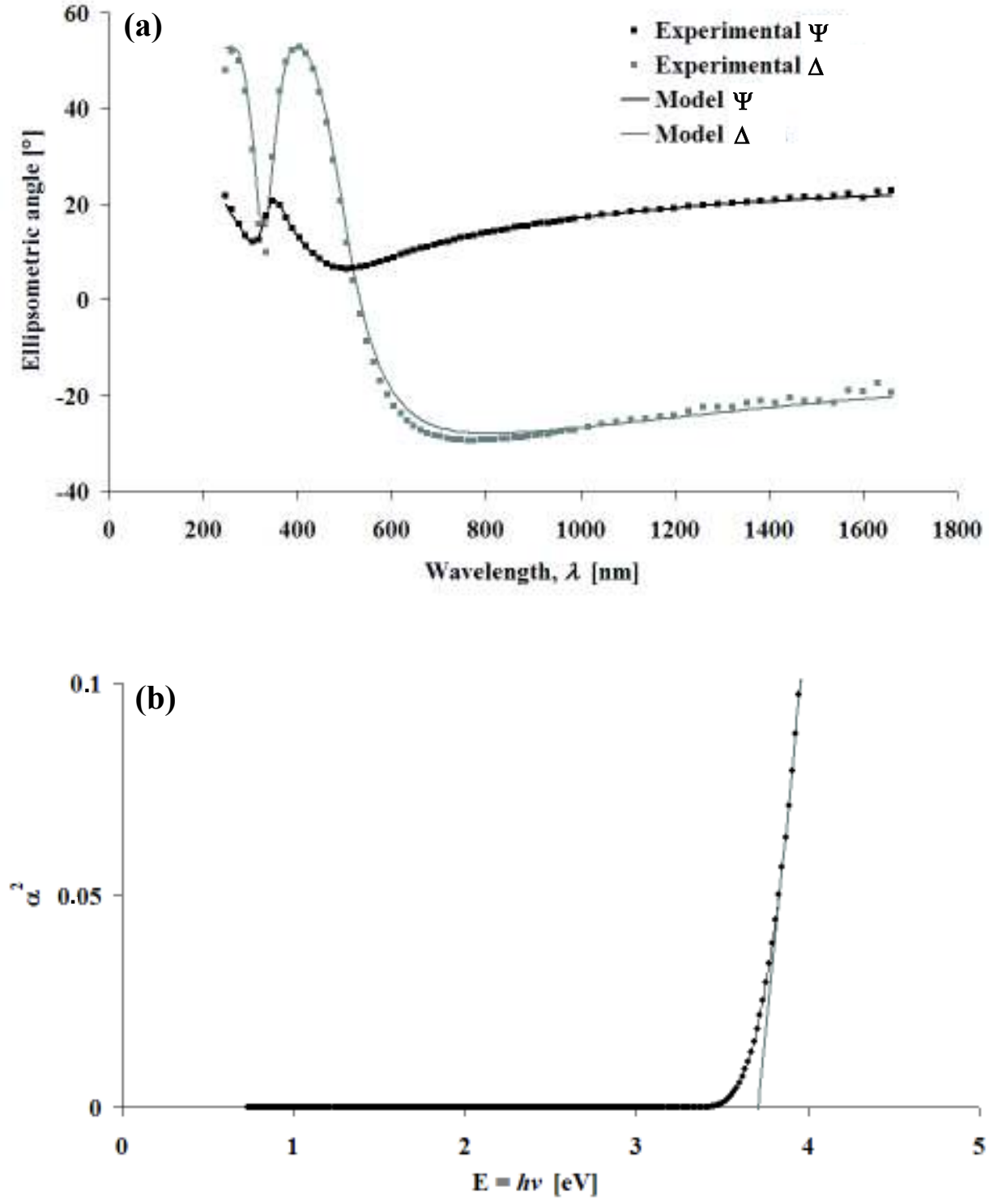

Figure(s)

# Figure 8

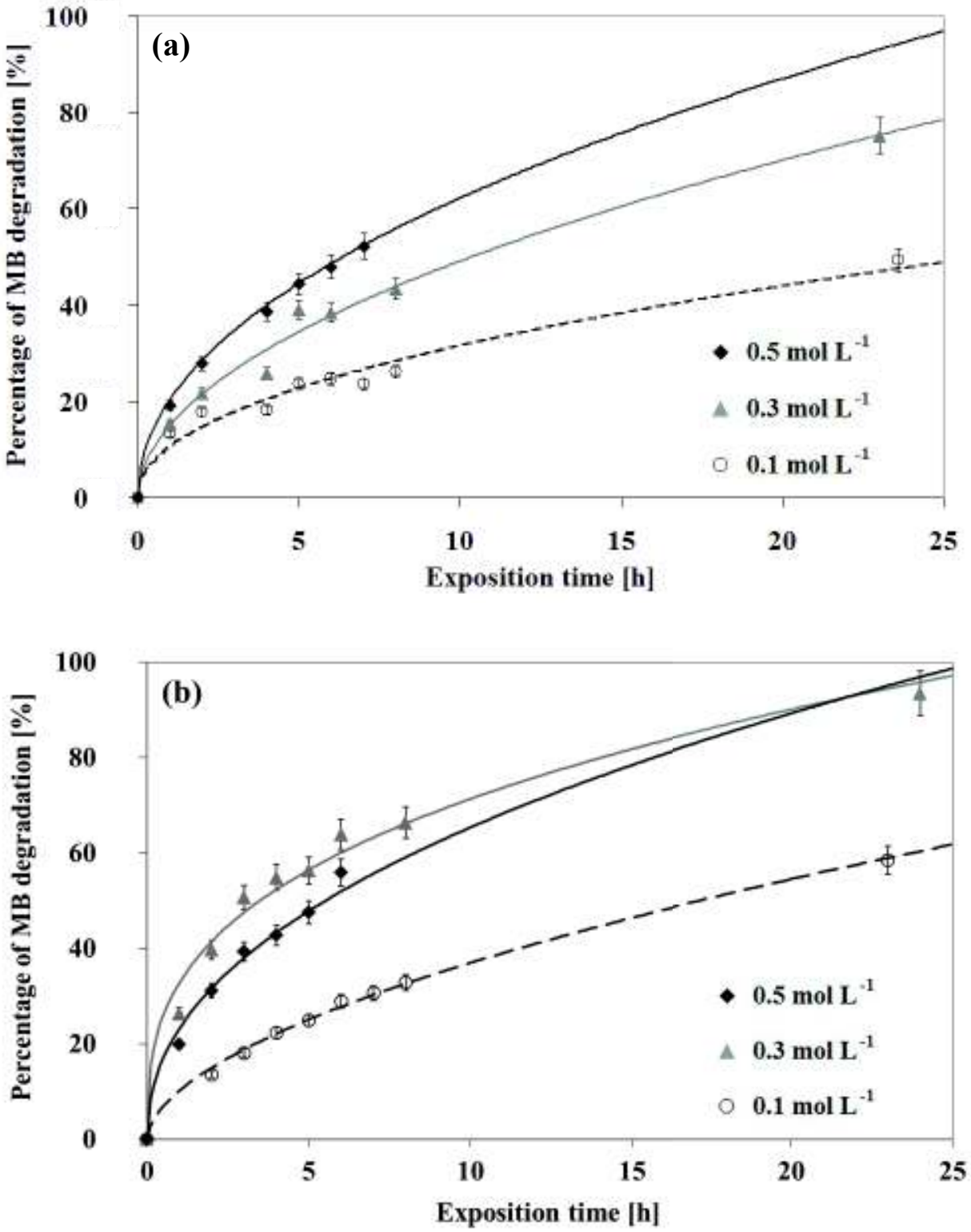

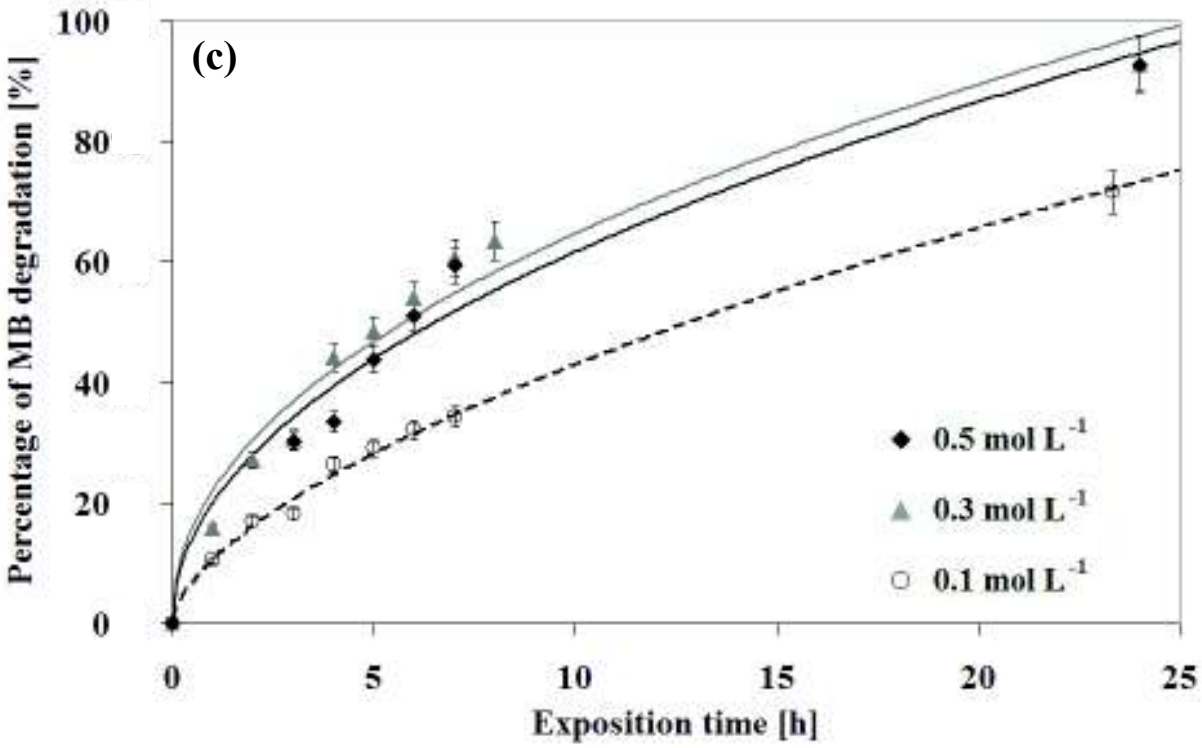
(c)
Percentage of MB degradation [%]
Exposition time [h]
0.5 mol L-1
0.3 mol L-1
0.1 mol L-1
0
20
40
60
80
100
0
5
10
15
20
25

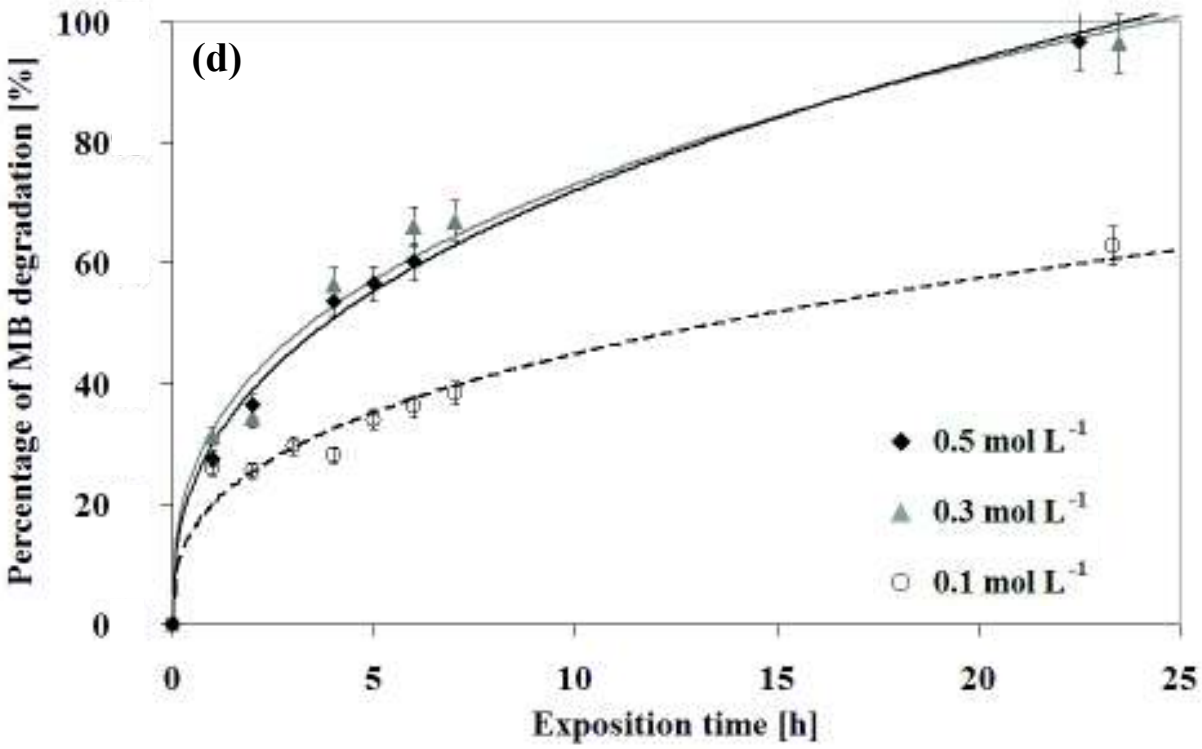
(d)
Percentage of MB degradation [%]
Exposition time [h]
0.5 mol L-1
0.3 mol L-1
0.1 mol L-1
0
20
40
60
80
100
0
5
10
15
20
25

Figure(s)

# Figure 9

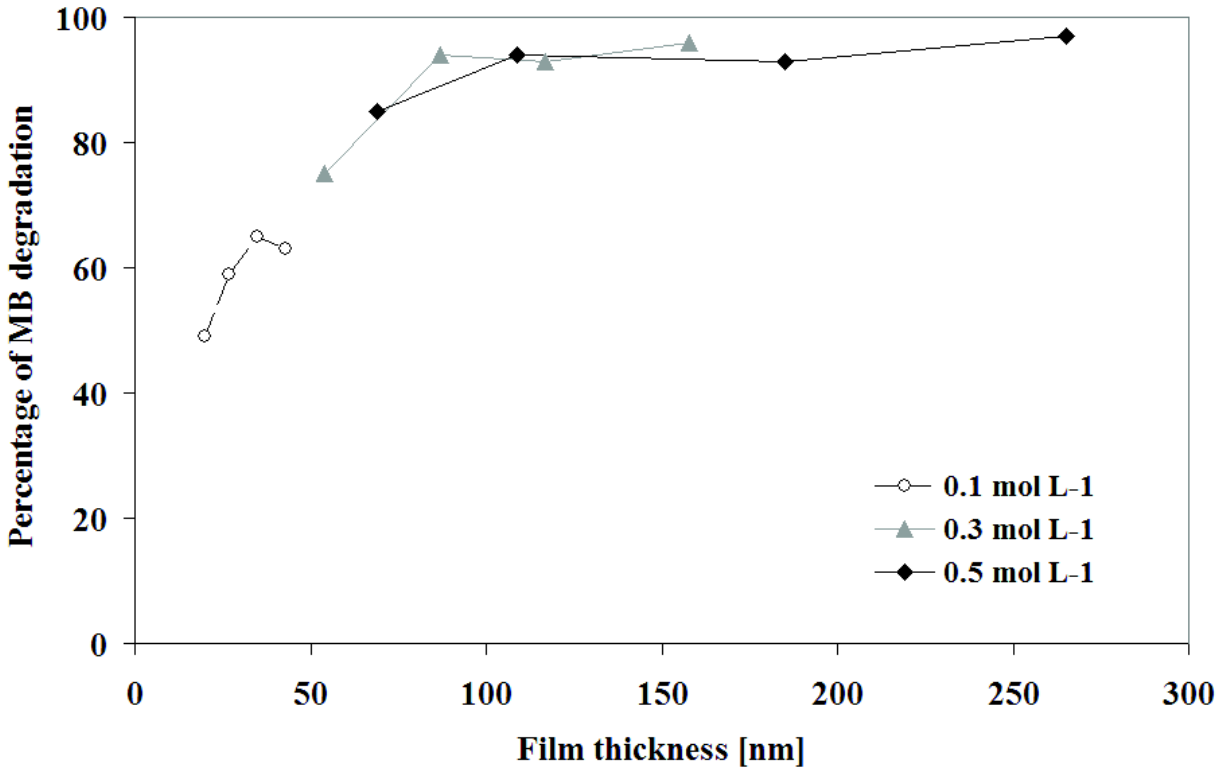

# Figure 10

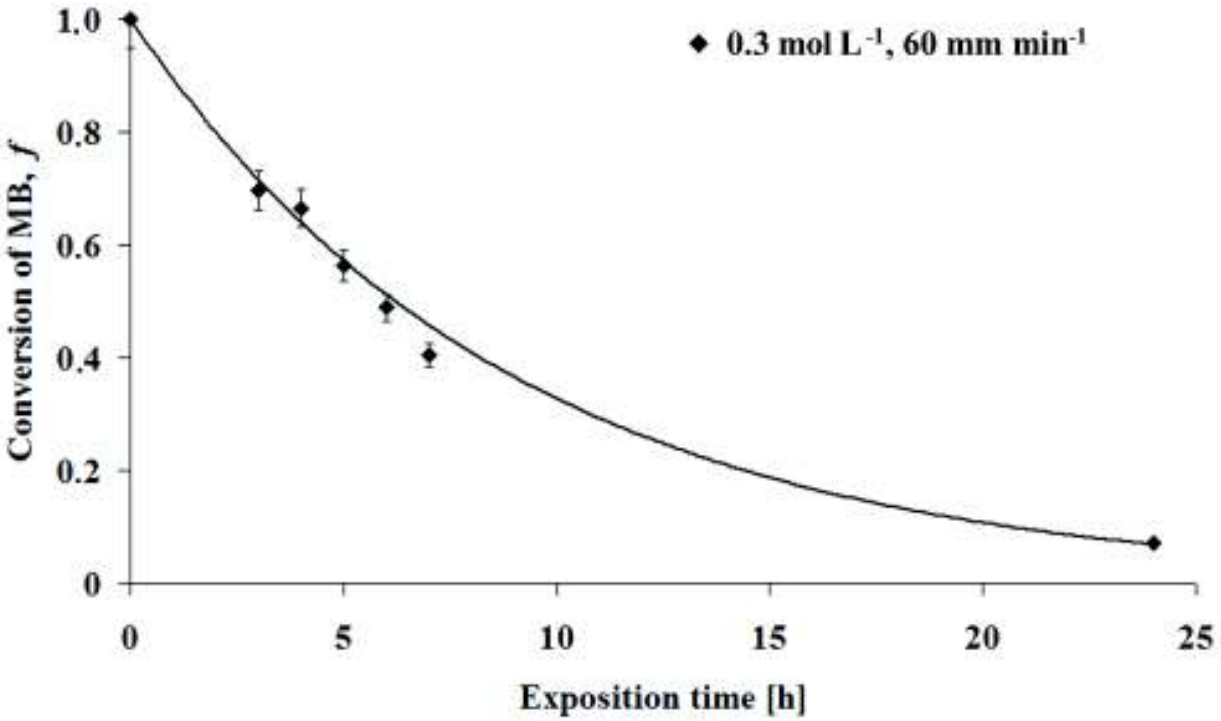
◆ 0.3 mol L-1, 60 mm min-1
Conversion of MB, f
1.0
0.8
0.6
0.4
0.2
0
0
5
10
15
20
25
Exposition time [h]

Figure(s)

# Figure 11

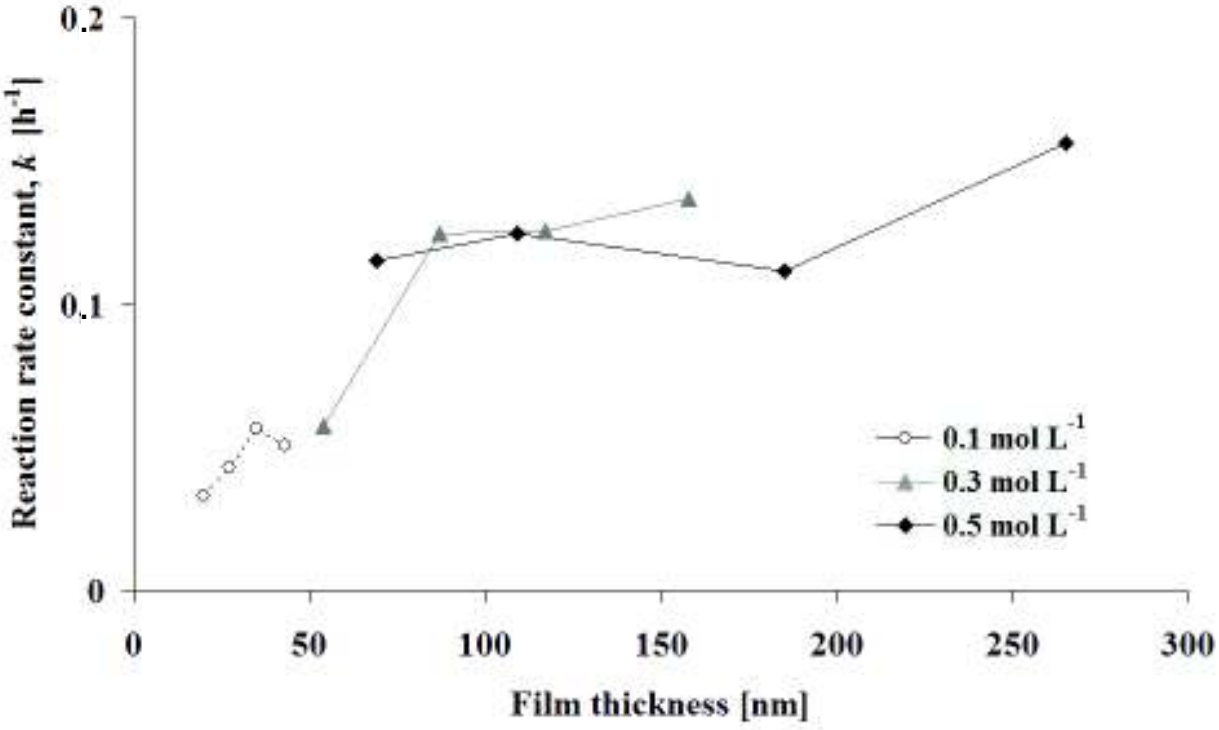

**Figure(s)**

Fig. 1: Experimental procedure for the production of single layer and multilayer films of $TiO_2$.

Fig. 2: Normalized XRD patterns of $TiO_2$ powders with [TTIP] = 0.1 – 0.3 – 0.5 mol $L^{-1}$ and calcined 1 h at 500°C compared to the reference pattern of $TiO_2$-anatase (ICDD file N°. 21-1272).

Fig. 3: (a) Normalized Kubelka–Munk function $F(R_\infty)$ calculated from DR-UV-Vis spectra and (b) transformed Kubelka–Munk function $(F(R_\infty)h\nu)^2$ of $TiO_2$ powders corresponding to [TTIP] = 0.1 – 0.3 – 0.5 mol $L^{-1}$ and calcined 1 h at 500°C.

Fig. 4: GIXRD patterns of $TiO_2$ thin films dipped one, two or three times (a) at 10 mm $min^{-1}$ and (b) at 90 mm $min^{-1}$ on alkaline free glass substrate and on soda-lime glass in a precursor solution [TTIP] = 0.5 mol $L^{-1}$ compared to the reference pattern of $TiO_2$-anatase (ICDD file N°. 21-1272).

Fig. 5: GIXRD patterns of single layer $TiO_2$ thin films on alkaline free glass substrate (a) dipped one time: (b) dipped three times with a speed of 90 mm $min^{-1}$ in precursor solutions of [TTIP] = 0.1 – 0.3 – 0.5 mol $L^{-1}$ compared to the reference $TiO_2$-anatase pattern.

Fig. 6: SEM micrographs for films dipped three times in a precursor solution of 0.5 mol $L^{-1}$ at (a) 10 mm $min^{-1}$, (b) 30 mm $min^{-1}$, (c) 60 mm $min^{-1}$ and (d) 90 mm $min^{-1}$.

Fig. 7: (a) Experimental and fitted ellipsometric angles $\Psi$ and $\Delta$ as functions of $\lambda$ and (b) evolution of $\alpha^2$ with h$\nu$ for a film dipped three times in a precursor solution [TTIP] = 0.5 mol $L^{-1}$ using alkaline free substrate and a withdrawing speed of 10 mm $min^{-1}$.

Fig. 8: Photocatalytic activities for the degradation of MB under UV light for $TiO_2$ films dipped three times at (a) 10 mm $min^{-1}$, (b) 30 mm $min^{-1}$, (c) 60 mm $min^{-1}$ and (d) 90 mm $min^{-1}$ in different sols corresponding to [TTIP] = 0.1 – 0.3 – 0.5 mol $L^{-1}$.

Fig. 9: Photocatalytic activities for the degradation of MB after 24 h under UV light as a function of the film thickness for $TiO_2$ films dipped three times in different sols ([TTIP] = 0.1 – 0.3 – 0.5 mol $L^{-1}$) and using different withdrawing speeds (10, 30, 60 and 90 mm $min^{-1}$).

Fig. 10: Experimental data and apparent first-order kinetic model for the conversion of MB under UV light as a function of the illumination time for a $TiO_2$ film dipped three times a sol corresponding to [TTIP] = 0.3 mol $L^{-1}$ and using a withdrawing speed of 60 mm $min^{-1}$.

Fig. 11: Reaction rate constant as a function of the film thickness for $TiO_2$ films dipped three times in different sols ([TTIP] = 0.1 – 0.3 – 0.5 mol $L^{-1}$) and using different withdrawing speeds (10, 30, 60 and 90 mm $min^{-1}$).